Significance of homologous temperature in softening behavior and grain size of pure metals processed by high-pressure torsion

Edalati, Kaveh
Department of Materials Science and Engineering, Faculty of Engineering, Kyushu University

Horita, Zenji
Department of Materials Science and Engineering, Faculty of Engineering, Kyushu University

出版情報：Materials Science and Engineering A. 528 (25/26), pp.7514-7523, 2011-09-25. Elsevier
バージョン：

Materials Science and Engineering A 528 (2011) 7514–7523
Received 30 December 2010, received in revised form 7 May 2011, accepted 25 June 2011.
Available online 2 July 2011.

Significance of homologous temperature in softening behavior and grain size of pure metals processed by high-pressure torsion

Kaveh Edalati*, Zenji Horita

Department of Materials Science and Engineering, Faculty of Engineering, Kyushu University, Fukuoka, Japan

Abstract
High purity metals with low melting temperatures such as indium (99.999%), tin (99.9%), lead (99%), zinc (99.99%) and aluminum (99.99%) were processed using high-pressure torsion (HPT). An unusual softening behavior was observed in all these metals after processing by HPT at room temperature. Pure copper (99.99%) and palladium (99.95%) were used to simulate the softening behavior due to a thermal effect by processing and subsequently holding at the temperatures equivalent to room temperature of pure Al. It is shown that a hardness peak appears in any metal by static softening after processing by HPT at a homologous temperature of 0.32 which is equivalent to room temperature of pure Al. The contribution of dynamic softening on hardness decrease becomes more important as the homologous temperature and stacking fault energy increase. Microstructural examinations indicate that, although the stacking fault energy influences the rate of the microstructural evolution, the homologous temperature appears to be a dominant parameter to determine the steady-state grain size after processing by HPT.
Keywords: Hardness; Grain size; High-pressure torsion; Ultrafine-grained materials; Severe plastic deformation.

* Corresponding author.
Tel.: +81 92 802 2992; fax: +81 92 802 2992.
E-mail address: kaveh.edalati@zaiko6.zaiko.kyushu-u.ac.jp (K. Edalati).

1. Introduction

Processing bulk metallic materials through the application of severe plastic deformation (SPD) leads to attainment of ultrafine-grained structures with a high hardness and strength [1–3]. Ighpressure torsion (HPT) is a typical process of SPD, where a thin disc or ring is placed between two massive anvils under a high pressure and intense shear strain is introduced by rotating the two anvils with respect to each other [4,5]. Application of HPT has shown that the microstructure as well as the hardness and strength evolve into a steady state with straining [6–18]. It has also been shown that the hardness after HPT processing is represented by a unique function of equivalent strain for various metals such as Al [5], Mg [19], Cu [20], Fe [21], Ti [22], Zr [23] and Hf [24].

The hardness-strain behavior of pure Al and Mg is different from other pure metals. In most metals, a steady level is reached directly following the initial increase with straining [5–24]. However, in pure Al with the purity level of 99.99% [5,25] and in pure Mg with the purity level of 99.9% [19], the hardness initially increases with increasing strain and, after reaching a maximum, decreases to a constant level. This softening of high purity Al at large equivalent strains was observed in both monotonic and cyclic HPT [26,27] as well as in continuous HPT [28]. The mechanism for the unusual softening of pure Al at large strains was investigated in few papers. Xu et al. [25] attributed the softening to easy cross-slip and dynamic recovery due to large stacking fault energy (SFE) of Al. Edalati et al. [29] reported that a hardness peak appears in Cu at a homologous temperature of 0.32 in a similar way to Al because of a static recrystallization, and the hardness behavior in pure Al was attributed to its relatively high homologous temperature [17]. It is noted that both Mg and Al are similar in terms of SFE and the melting temperature. If the effect of SFE is dominant, a softening should be observed in pure metals with high SFE such as Pd and if the effect of homologous temperature is dominant a softening should be observed in pure metals with low melting temperatures such as In, Sn, Pb and Zn. Therefore, the hardness behavior of these metals is examined in this paper, for the first time, after processing by HPT.

The grain size of pure Al and Mg at the steady-state is also different from that of other pure metals. In pure Al with the purity level of 99.99%, the average grain size at the steady state was reported 1.2 μm [14], 1.5 μm [4], 1.9 μm [17] and 2.1 μm [16]. In pure Mg with the purity level of 99.9%, the average grain size at the steady state was reported 1.0 μm [19]. However, in other metals, the steady-state grain size is in the submicrometer level [7–24]. Although the larger grain size in Al is attributed to its high SFE [5,25] or to its low melting temperature [29], little is understood to date regarding the relation between the steady-state grain size and SFE or melting temperature of pure metals processed with HPT. Mohamed [30] investigated the correlations between the minimum grain size at the steady state and physical parameters for pure metals processed through ball milling using a dislocation model. However, this finding cannot be applied directly to HPT-processed pure metals because the mechanism of grain refinement is not the same for ball milling and HPT processing.

This study is thus initiated with the two objectives: first, to examine the possible softening behavior in HPT-processed pure metals such as In, Sn, Pb, Zn, Al, Cu, Ni and Pd and clarify the reason for the difference in the hardness behavior; and second, to investigate the effect of

homologous temperature and SFE on the grain size at the steady state.

2. Experimental materials and procedures

High purity In (99.999%), Sn (99.9%), Pb (99%), Ni (99.996%) and Pd (99.95%) were received in a form of cold-rolled plates having dimensions of 1 mm × 25 mm × 50 mm for In, Sn and Ni, 1.5 mm × 50 mm × 100 mm for Pb and 0.3 mm × 25 mm × 30 mm for Pd. High purity Zn (99.99%) was received in a form of ingot having dimensions of 20 mm × 50 mm × 120 mm and high purity Al (99.99%) and Cu (99.99%) were received in a form of cold-extruded rods with 10 mm diameter and 1250 mm length. Discs with 10 mm diameter and 0.8 mm thickness were prepared from the plates and rods using either of a wire-cutting electric discharge machine, a micro-cutter or scissors. For In, Sn, Pb, Zn, Al, Cu and Ni, the discs were ground to a thickness of 0.8 mm. For Pd, every three discs with 0.3 mm thickness were compressed together and the total thickness of 0.9 mm was reduced to 0.8 mm. The discs with 0.8 mm thickness were annealed for 1 h at a temperature in the range of 0.6–0.92 T_m (T_m: melting temperature) which is considered to be in the high temperature regime. The discs were annealed at 393 K for In, 453 K for Sn, 473 K for Pb, 523 K for Zn, 773 K for Al, 873 K for Cu, 973 K for Ni and 1273 K for Pd to give an initial grain size of ~350 μm for In, ~590 μm for Sn, ~160 μm for Pb, ~1220 μm for Zn, ~1050 μm for Al, ~150 μm for Cu and Ni, and ~50 μm for Pd. The crystal structure of these elements, including their purity, melting temperature T_m, homologous temperature corresponding to room temperature $298/T_m$, and SFE, are given in Table 1. The data in Table 1 were taken from Refs. [31–33].

Table 1. Purity, crystal structure, melting point T_m, homologous temperature corresponding to room temperature $298/T_m$, and stacking fault energy SFE, for various elements.

Metal	**Purity** (%)	**Structure**	T_m (K) [31]	$298/T_m$	**SFE** ($mJ.m^{-2}$) [32, 33]
In	99.999	Tetragonal	429	0.69	
Sn	99.9	Tetragonal	505	0.59	
Pb	99	fcc	600	0.50	24.5
Zn	99.99	hcp	693	0.43	140
Al	99.99	fcc	933	0.32	166
Cu	99.99	fcc	1357	0.22	45
Ni	99.996	fcc	1728	0.17	125
Pd	99.96	fcc	1825	0.16	180

HPT was conducted at room temperature (298 K) using the In, Sn, Pb, Zn and Al discs for either N = 0.25, 1, 2 or 5 revolutions, at temperatures of 298 K, 373 K, 433 K, 473 K, 513 K, 543 K and 573 K using the Cu discs for N = 12 revolutions, at temperatures of 298 K and 573 K using the

Pd discs for 15 revolutions and at temperatures of 298 K using the Ni discs for 10 revolutions. A pressure of P = 1 GPa was applied on In, Sn, Pb and Al discs and a pressure of P = 2 GPa was applied on Zn, Cu, Ni and Pd discs, while rotating with a speed of ω = 0.5 rpm. The details concerning the HPT anvils were reported elsewhere [23]. The Cu and Pd discs, after processing with HPT at elevated temperatures, were held at the same temperature as the HPT processing temperature for a period of 30 h, as described in an earlier paper [29].

Following HPT and after keeping the samples for duration time of 30 h, the discs were subjected to Vickers microhardness measurement and evaluated using optical microscopy (OM), electron back-scatter diffraction (EBSD) analysis and transmission electron microscopy (TEM).

First, the HPT-processed discs including the annealed discs were polished to mirror-like surfaces and the Vickers microhardness was measured at selected points from the center to periphery, using the procedure described earlier [20]. The microhardness was measured with an applied load of 10 g on In, Sn and Pb discs, of 50 g on Zn and Al discs and of 200 g on Cu, Ni and Pd discs for duration time of 15 s. The equivalent strain, ε, at each hardness measurement was calculated as [7]:

$$\varepsilon = \frac{2\pi r N}{\sqrt{3}\ t} \qquad (1)$$

where r is the distance from the disc center, N is the number of revolutions and t is the thickness of disc. The thickness reduction during HPT processing and the slippage between the anvils and sample were ignored in the calculation of the equivalent strain in this study [21,34].

Second, for OM observations, the In, Sn and Pb discs were polished to mirror-like surfaces and the In discs were electro-etched in a solution of 5% HF and 95% H_2O at 298 K under an applied voltage of 15 V; the Sn discs were etched in a solution of either 5% HCl and 95% CH_3OH or 5% HNO_3 and 95% C_2H_5OH at 298 K; and the Pb discs were etched in a solution of 5% HNO_3 and 95% C_2H_5OH at 298 K or electro-etched using a solution of 30% $HClO_4$ and 70% CH_3COOH at 298 K under an applied voltage of 5 V. The etched samples were observed using OM for microstructural observation.

Third, for EBSD analysis, the Zn, Al, Cu and Pd discs were polished to mirror-like surfaces and further subjected to electro-chemical polishing in a solution of 50% $HClO_4$ and 50% C_2H_5OH at 298 K under an applied voltage of 5 V for Zn; 15% $HClO_4$, 15% $C_3H_5(OH)_3$ and 70% CH_3OH at 263 K under an applied voltage of 13 V for Al; 15% HNO_3, 15% $C_3H_5(OH)_3$ and 70% CH_3OH at 263 K under an applied voltage of 9 V for Cu; and 50% HCl, 20% $C_3H_5(OH)_3$ and 30% C_2H_5OH at 298 K under an applied voltage of 20 V for Pd. EBSD analysis was performed at a voltage of 20 kV and the crystal orientations were determined using an automatic beam scanning system. The EBSD probe size for Zn, Al, Cu and Pd was 150 nm, 100 nm, 90 nm and 70 nm, respectively.

Fourth, for TEM, discs with 3 mm in diameter were punched from the Al, Cu, Ni and Pd discs at 3.5 mm away from the center. The 3 mm discs were ground to a thickness of 0.15 mm and further thinned for transmission electron microscopy (TEM) with a twin-jet electro-chemical polisher using the solutions as mentioned above for Al, Cu and Pd. Thin specimens for Ni were made in the same way using a solution of 10% HSO_4, 10% HNO_3 and 80% CH_3OH at 263 K under an applied voltage

of 20 V. TEM was performed at a voltage of 200 kV for microstructural observation and for recording selected-area electron diffraction (SAED) patterns.

The average size of grains separated by large misorientation angles was determined by either OM, EBSD or TEM observations. For, OM and EBSD, the average grain sizes were determined by the linear intercept method. For TEM, the grain size values were obtained by measuring the two orthogonal axes of the bright areas in the dark field images. More than 50 grains were calculated for each group of samples. The low-angle grain boundaries were excluded in the measurements and the twin boundaries which were present in some elements were considered as grain boundaries.

3. Results

The hardness values measured at room temperature (0.32 T_m) are plotted against the equivalent strain in Fig. 1 for Al. Data points fall well on a single curve in consistence with earlier studies [5,6,26–29]. The hardness of Al initially increases to a maximum, decreases with a further increase in the equivalent strain and reaches a steady state level where the hardness remains unchanged with straining. Despite the fact that the equivalent strain is theoretically zero at the center of disc according to Eq. (1), close inspection of Fig. 1 reveals that the hardness at the disc center increases with increasing the number of revolutions. This is due to two reasons [21]: first, in practice, hardness measurement at the exact center is difficult but the hardness values were measured within a circular area with 0.2 mm in diameter; second, a small misalignment of the rotation axes between the lower and upper anvils may result in imposing an additional shear strain to the center of the disc, although the alignment was adjusted well within ±0.01 mm in this study. Microstructures at the steady states are shown in Fig. 2 for Al, where (a) is a TEM bright-field image and (b) is an orientation map obtained by EBSD. Few dislocations are visible and grain boundaries are straight and well defined with a grain size of ~1.9 μm. These microstructural features are also consistent with earlier observations for HPT-processed samples [5,6,29]. However, the average grain size is higher than the grain size of ~1.2 μm reported for samples processed with equal-channel angular pressing [35,36].

The hardness is plotted against the equivalent strain in Fig. 3 for Zn processed at room temperature (0.43 T_m). As in Al, the hardness of Zn initially increases and after reaching a maximum decreases to a steady state level. Orientation map analysis using EBSD is shown in Fig. 4 for the sample processed for N = 1 revolution at three representative strained conditions. Here, (a) corresponds to the center of disc, ε = 0, where the hardness increases; (b) corresponds to 1 mm away from the disc center, ε = 4, where the hardness takes the maximum; (c) corresponds to 3 mm away from the disc center, ε = 13, where the hardness reaches a steady state. It is apparent from Fig. 4(a) that at ε = 0, the microstructure consists of large grains. In Fig. 4(b) where ε = 4, the grains become smaller and low quality of image indicates that the lattice strain should be high. In Fig. 4(c) where ε = 13, small grains with straight and well-defined grain boundaries appear and the grains size reaches ~5.2 μm. These microstructural features of Zn at different strained conditions are similar to the earlier observation of Al [6] and Mg [19] and different from those of Cu [9] and Fe [10].

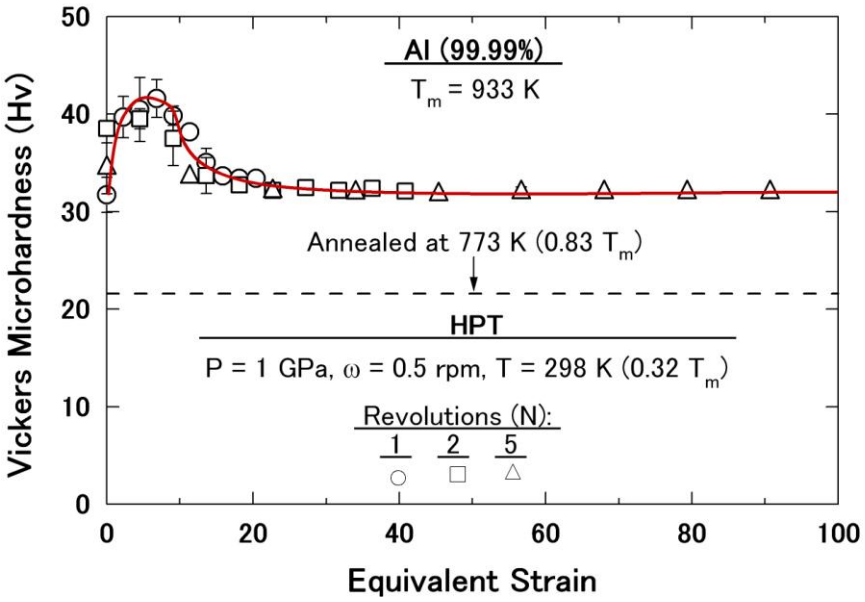

Fig. 1. Vickers microhardness plotted against equivalent strain for Al after HPT at room temperature.

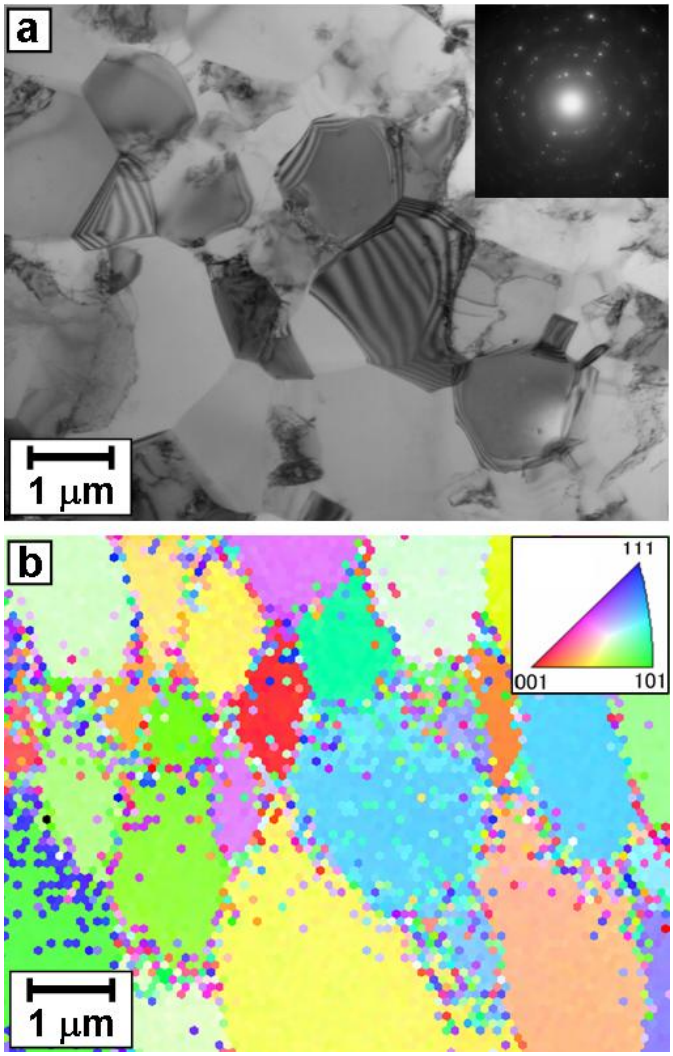

Fig. 2. (a) TEM bright-field image and SAED patterns and (b) EBSD orientation map for Al after HPT for 5 revolutions at room temperature.

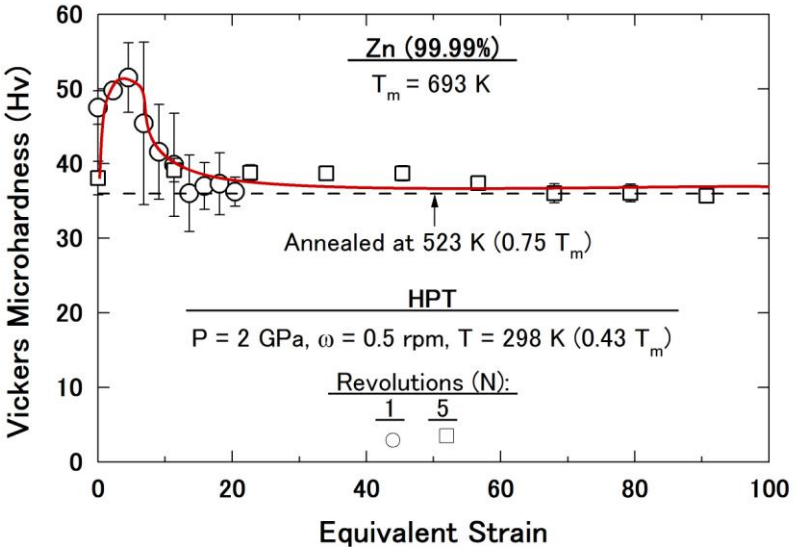

Fig. 3. Vickers microhardness plotted against equivalent strain for Zn after HPT at room temperature.

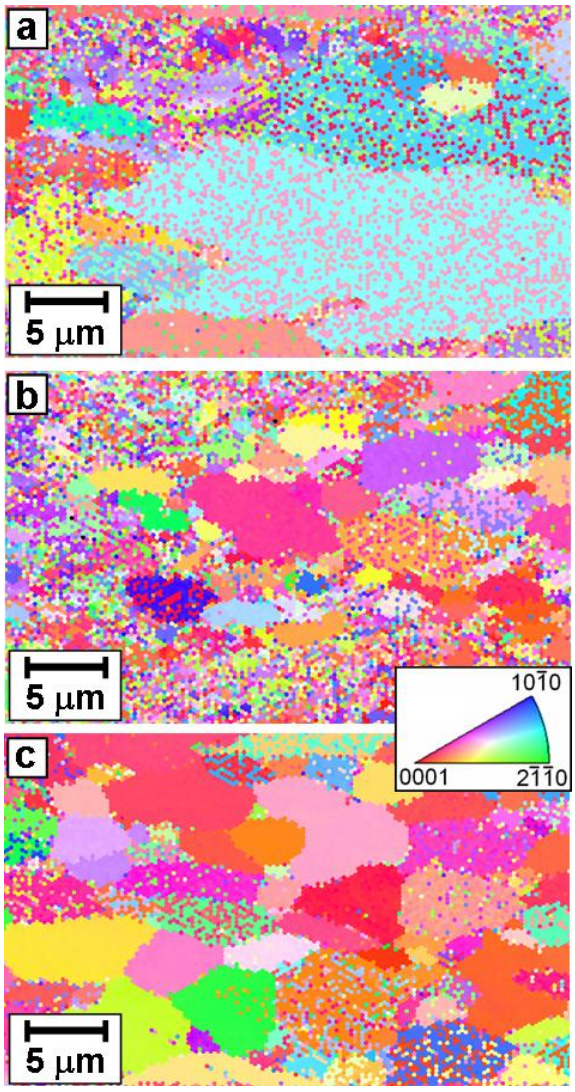

Fig. 4. EBSD orientation map for Zn after HPT for 1 revolution at room temperature at (a) disc center, (b) 1 mm from center and (c) 3 mm from center.

The hardness is plotted against the equivalent strain in Fig. 5 for (a) Pb, (b) Sn and (c) In processed at room temperature (0.43, 0.59 and 0.69 T_m for Pb, Sn and In, respectively). There are two points to be noted regarding the plots in Fig. 5. First, although the hardness behavior is similar to Al and Zn and the average hardness is higher in the strain range of $\varepsilon < 20$ than that of $\varepsilon > 20$, the hardness variation with straining is insignificant in these three metals. Second, the hardness values measured after processing at room temperature are unusually lower than those annealed at elevated temperatures prior to HPT processing. For Al, as shown in Fig. 1, the hardness level at the steady state is higher than that of the annealed sample and, for Zn, it is almost the same as the hardness level of the annealed sample as shown in Fig. 3.

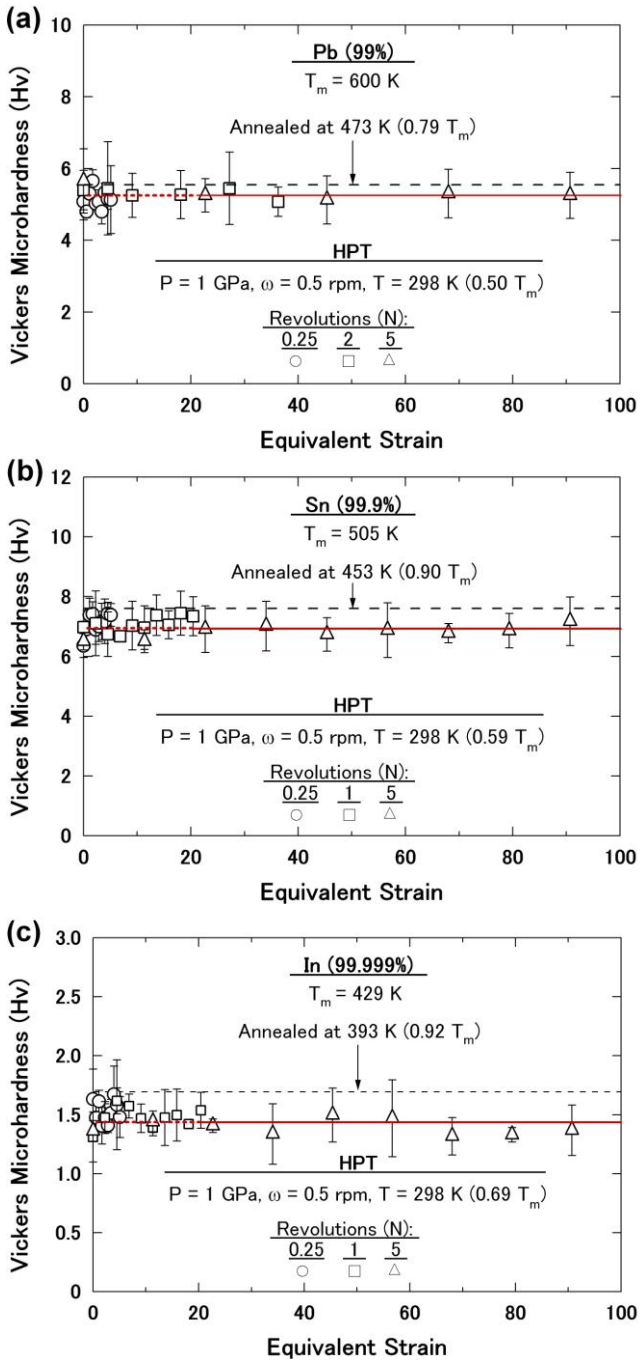

Fig. 5. Vickers microhardness plotted against equivalent strain for (a) Pb, (b) Sn and (c) In after HPT at room temperature.

OM Micrographs are shown in Fig. 6 for (a, b) Pb, (c, d) Sn and (e, f) In, where (a), (c) and (e) were taken from the annealed samples and (b), (d) and (f) were taken from the samples subjected to HPT at room temperature for N = 5 revolutions at 3.5 mm away from the disc center. It is shown that the microstructures consist of large grains and, whereas some twins are visible in Pb and In, they are rarely seen in Sn. The average grain sizes of Pb, Sn and In appear to be ~160, ~590 and ~350 μm after annealing and they are compared with ~100, ~135 and ~320 μm after processing by HPT, respectively. These grain sizes at the steady state are much higher than any other reported sizes for SPD-processed materials [1–29]. It is noted that despite a moderate decrease in the grain size after the HPT processing, the hardness decreases slightly by HPT.

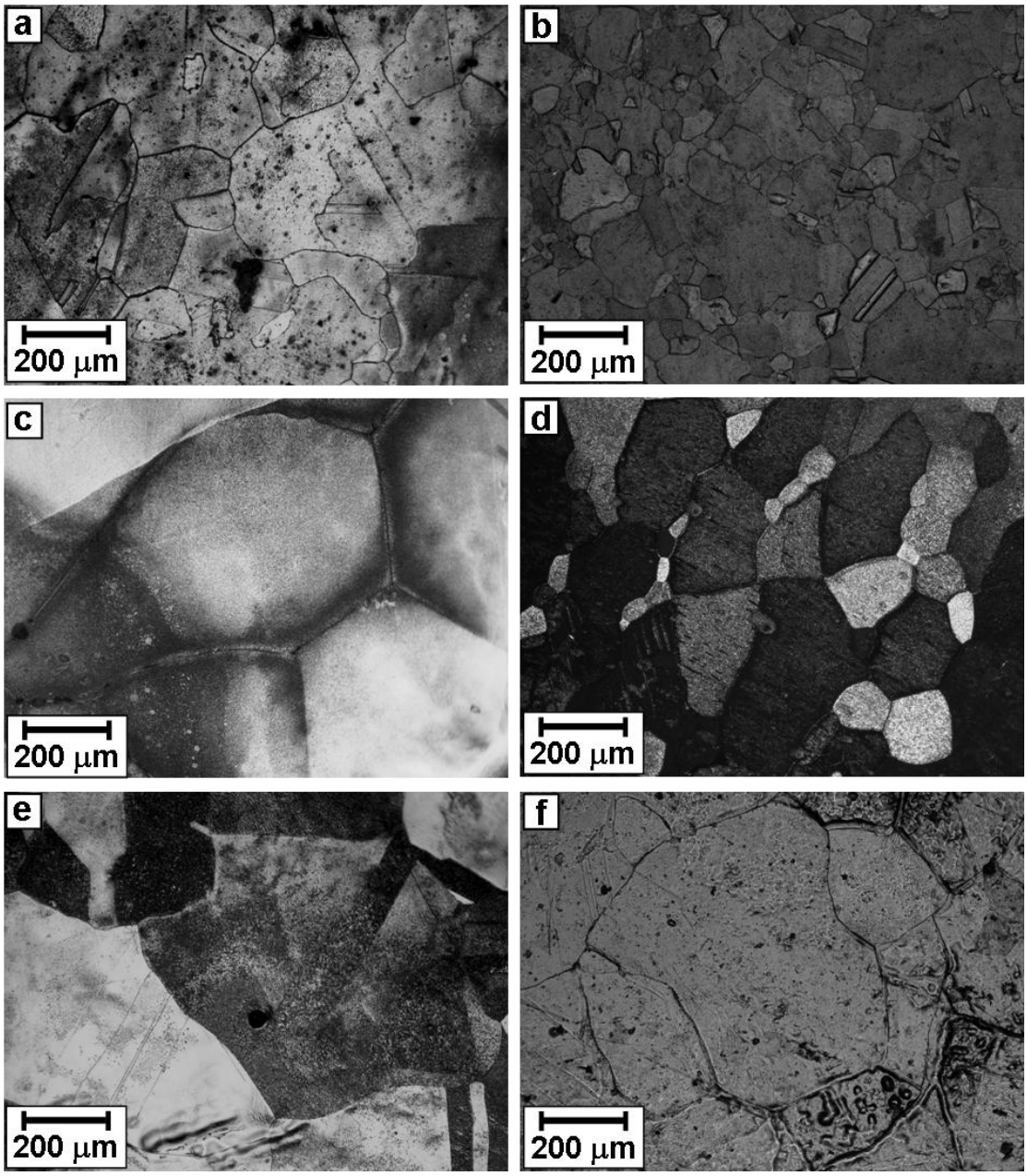

Fig. 6. Micrographs of (a, b) Pb, (c, d) Sn and (e, f) In observed using optical microscopy, where (a), (c) and (e) are after annealing for 1 h and (b), (d) and (f) are after HPT for 5 revolutions at room temperature.

4. Discussion

Because significant numbers of dislocations are generated as a consequence of intense straining through HPT processing, it is reasonable to consider that the difference in the hardness variation and microstructural feature arises from the difference in dislocation behavior between the metals. It is most probable that four important factors affect the dislocation behavior in pure metals: they are first the purity level, second the crystal structure, third the homologous temperature, and forth the SFE. The purity level is an important factor affecting the dislocation mobility, but this effect can be the same for all elements adopted in this study and in the earlier studies of Mg [19], Cu [20], Fe [21], Ti [22], Zr [23] and Hf [24], because all these selected metals have almost the same purity level. Since the softening behavior is observed for different crystal structures such as tetragonal (In, Sn), fcc (Al, Cu, Pd) and hcp (Mg, Zn), the behavior must be common to any crystal structures. This study thus examines possible effects of the two other factors, the homologous temperature and the SFE, on the hardness behavior and the grain size after HPT.

4.1. Effect of homologous temperature on hardness behavior

Although HPT was conducted at room temperature (298 K) for all selected metals in this paper such as In, Sn, Pb, Zn and Al as well as for the metals studied in the earlier papers such as Mg [19], Cu [20], Fe [21], Ti [22], Zr [23] and Hf [24], the temperature of 298 K corresponds to different homologous temperatures varied from 0.12 for Hf [24] to 0.69 for In. Thus, the dislocation mobility including the behavior of recovery and recrystallization should be different between the individual metals. Here, the pure Cu was processed at a selected temperature in the range of 298–573 K (0.22–0.42 T_m) to simulate a thermal effect on the hardness behavior in pure metals. Furthermore, it is important to consider that the discs subjected to HPT at room temperature are kept for some periods of time before hardness measurement and microstructural observation. Therefore, the HPT-processed Cu discs at elevated temperatures were kept at the same corresponding temperatures for 30 h.

Fig. 7(a) plots the hardness variation with the equivalent strain for Cu discs processed for N = 12 revolutions at different temperatures. The hardness variations at elevated temperatures are essentially the same as the one at room temperature as reported in an earlier paper [20] and no hardness peak is observed at the selected temperatures. Now the major difference is that the steady state level decreases with an increase in the processing temperature. Thus, this indicates unambiguously that dynamic softening (due to recovery and/or recrystallization) occurs during HPT. In order to simulate the static softening after processing by HPT, the HPT-processed Cu discs at elevated temperatures were annealed at the same corresponding temperatures for 30 h. The hardness values are then plotted against the equivalent strain in Fig. 7(b) for different processing temperatures. It is now apparent that a hardness maximum appears at homologous temperatures higher than 0.27 and such a maximum is shifted to lower equivalent strain as the homologous temperature increases. Furthermore, the hardness level at the steady state is decreased with the post-HPT annealing. In accordance with an earlier study [29], the hardness peak appears by static softening after processing by HPT in Cu.

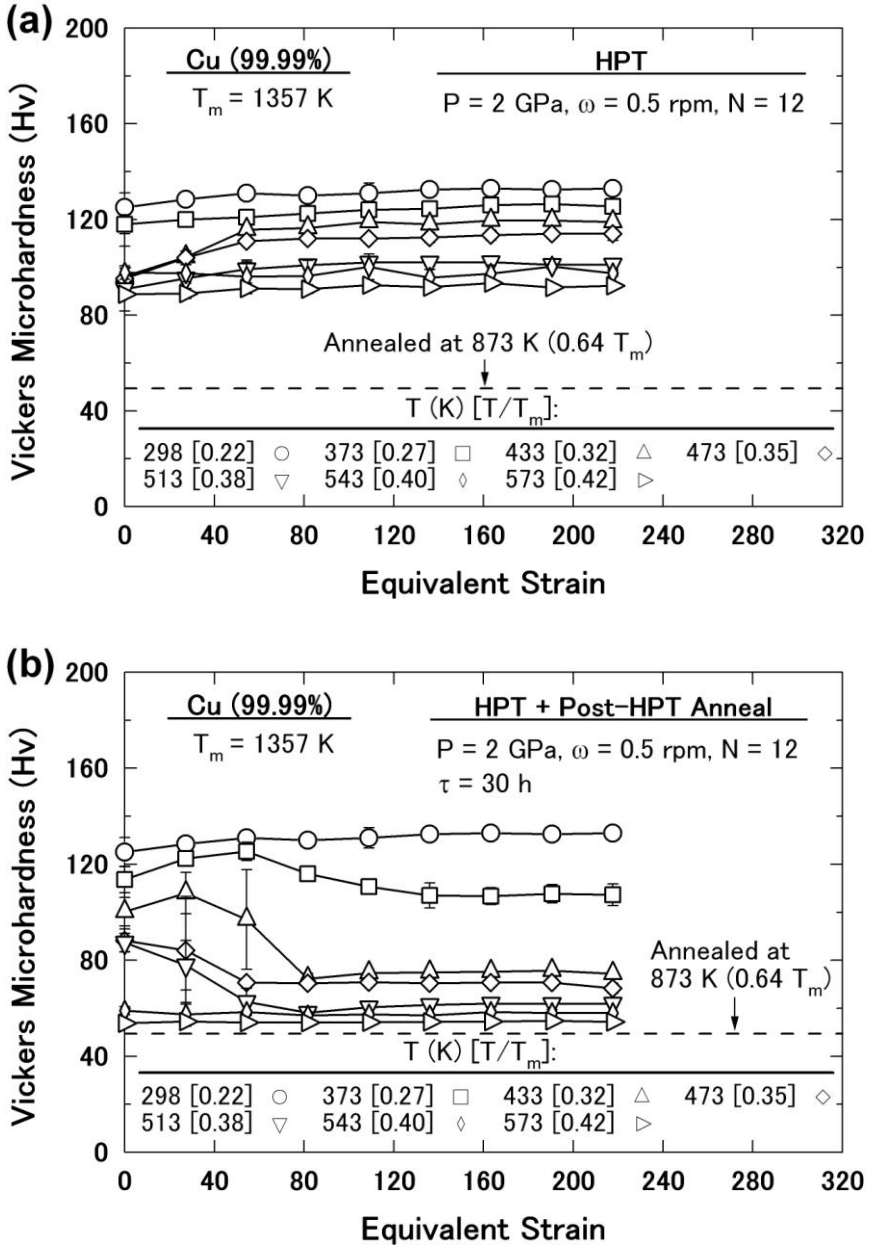

Fig. 7. Vickers microhardness plotted against equivalent strain for Cu after (a) HPT at various temperatures for 12 revolutions and (b) post-HPT annealing at the same corresponding temperature to HPT for 30 h.

The contribution of dynamic softening to the hardness decrease at a temperature of T with respect to room temperature, R_D, may be estimated as

$$R_D = \frac{HV_{RT} - HV_T}{HV_{RT} - HV_{PA}} \times 100 \qquad (2)$$

where HV_{RT} is the hardness after processing by HPT at room temperature, HV_T is the hardness after processing by HPT at a temperature of T and HV_{PA} is the hardness after post-HPT annealing at a temperature of T. Considering the hardness values at the steady states in Fig. 7(a) and (b), R_D values are then estimated and plotted against the homologous temperature in Fig. 8. This plot indicates that the contribution of dynamic softening to the hardness decrease becomes more important as the

homologous temperature increases. Therefore, the dynamic softening is expected to be the dominant mechanism for the softening behavior in low-melting metals such as Pb, Sn and In. Extrapolating the data points for Cu in Fig. 8 to an homologous temperature of 0.5 results in R_D = 70%.

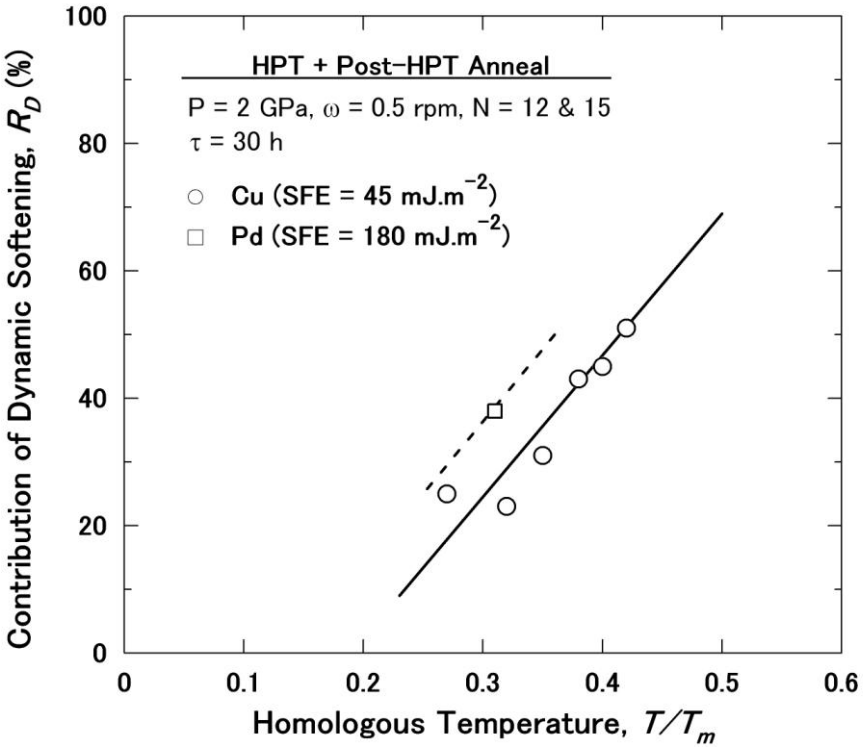

Fig. 8. Contribution of dynamic softening, R_D, plotted against homologous temperature, T/T_m, for Cu and Pd.

Microstructures including SAED patterns are shown in Fig. 9 for Cu after HPT processing at 433 K for (a, b) N = 1, (c, d) N = 4 and (e, f) N = 12 revolutions and post-HPT annealing at 433 K for 30 h. Panels (a), (c) and (e) in Fig. 9 are TEM bright-field images, panels (b) and (d) in Fig. 9 are TEM dark-field images taken with the diffracted beams indicated by an arrow in the SAED patterns and (f) is an orientation map by EBSD. The temperature of 433 K was selected because it is 0.32 T_m for Cu and is equivalent to the room temperature for Al. It is noted that N = 1 revolution corresponds to ε = 16 where the hardness increases, N = 4 to ε = 60 where the hardness takes the maximum, and N = 12 to ε = 190 where the hardness reaches a steady state. Many dislocations are visible within grains in Fig. 9(a)–(d), and grain boundaries are ill-defined. The grain size is fairly reduced to 2.9 μm in Fig. 9(e) and (f). The microstructure at the steady state contains few dislocations as shown in Fig. 9(e) and many twins are visible in the grains. These are typical features observed after annealing of deformed fcc metals with low SFE. These microstructural features of Cu at different strained conditions are similar to those of Zn as shown in Fig. 4 as well as to the earlier observation of Al [6] and Mg [19]. All these results suggest the importance of homologous temperature in softening behavior of pure metals.

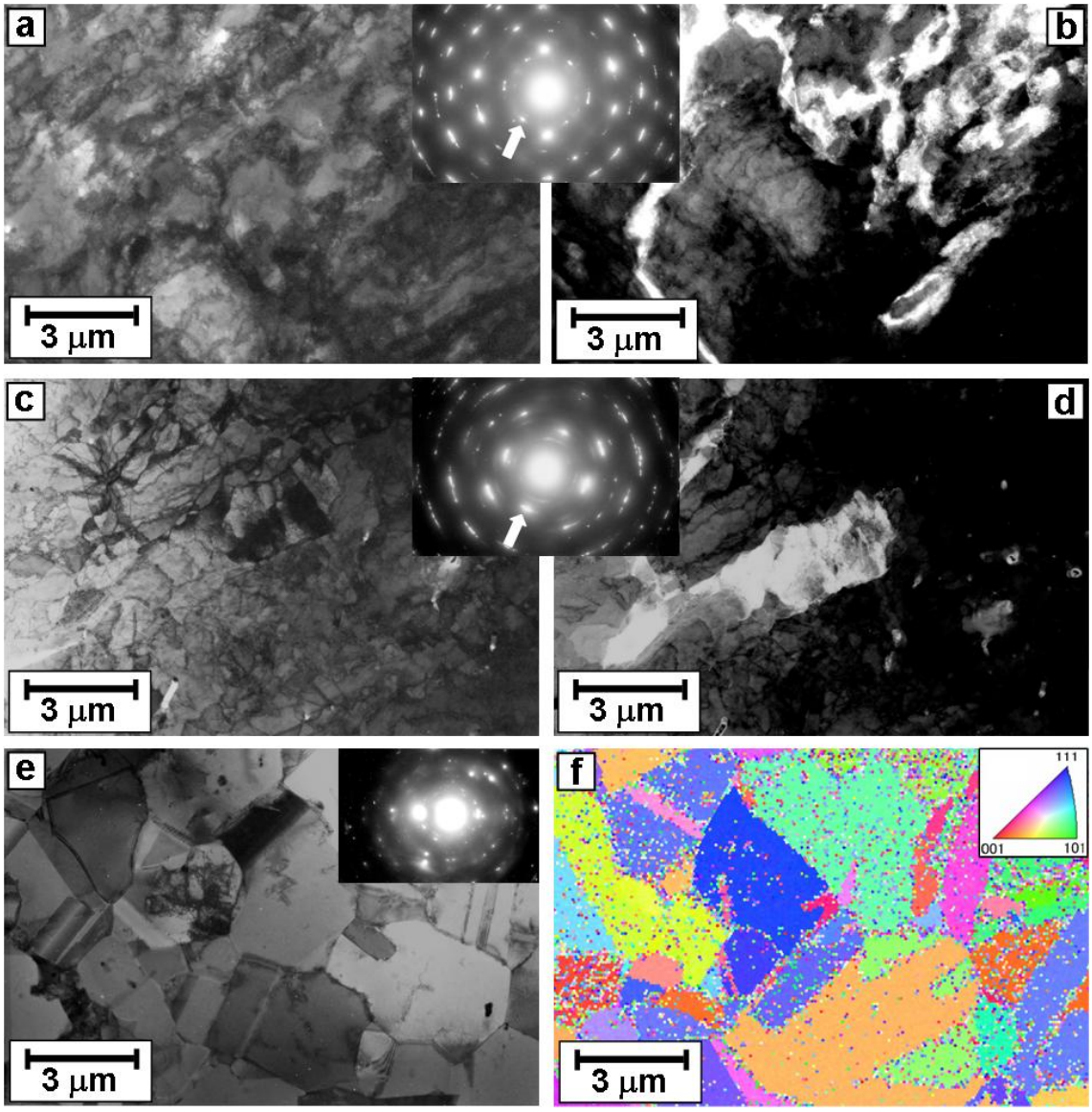

Fig. 9. (a)–(e) TEM micrographs and SAED patterns and (f) EBSD orientation map for Cu after HPT processing at 433 K for (a, b) 1, (c, d) 4 and (e, f) 12 revolutions and post-HPT annealing at 433 K for 30 h, where (b) and (d) are dark-field images of (a) and (c), respectively, taken with the diffracted beams indicated by arrows in SAED pattern.

4.2. Effect of stacking fault energy on hardness behavior

It is thus clearly demonstrated that static recrystallization occurs after HPT processing of Cu when the temperature for HPT and subsequent holding of the sample becomes equivalent to the room temperature as in Al and Mg (T = 0.32 T_m) and Zn (T = 0.42 T_m). The results of Cu are then well consistent with those of Al, Mg and Zn. However, it is important to examine the effect of SFE on the hardness behavior and microstructural feature along with HPT operation because, as given in Table 1, the SFE is large as 166 mJ m^{-2} for Al, 125 mJ m^{-2} for Mg and 140 mJ m^{-2} for Zn, but is small as 45 mJ m^{-2} for Cu [32]. It is well known that the dislocation mobility is assisted with two main mechanisms: cross-slip and climb. The controlling factor for cross-slip is SFE as well as

homologous temperature and the controlling factor for climb is lattice self-diffusion and homologous temperature. In contrast to cubic metals, the cross-slip is very difficult to occur in hcp metals because of crystallographic anisotropy and limited slip systems. Therefore, the climb should be the main mechanism for softening of strain-hardened hcp Zn, which is mainly controlled by the homologous temperature. However, in fcc metals, it is well established that the distance between the two dissociated partial dislocations is small when SFE (SFE/*Gb*, where *G* is the shear modulus and *b* is the Burger vector) is large and the smaller distance promotes the dislocation mobility through cross-slip mechanism as for the case of Al. The reverse is applicable so that the dislocation mobility is low when SFE is small as in Cu. Consequently, the microstructure evolves much faster in Al when compared to Cu. Therefore, the softening may even proceed dynamically during HPT as suggested by Xu et al. [25].

In order to clarify the effect of SFE on softening behavior, pure Pd was used to simulate a thermal effect on the hardness behavior and microstructural evolution of pure Al. As given in Table 1, the SFE is 180 mJ m^{-2} for Pd which is close to 166 mJ m^{-2} for Al [32]. As attempted in the Cu case, this simulation consists of processing and subsequently holding the pure Pd at 573 K (0.31 T_m), which is equivalent to room temperature for pure Al.

Fig. 10(a) plots the hardness variation with the equivalent strain for Pd discs processed at the temperatures of 273 K (0.16 T_m) and 573 K (0.31 T_m) for N = 15 revolutions. Despite the high SFE for Pd, the hardness variations are essentially the same as pure Cu and no maximum appears in the plots of both temperatures. The differences are that the steady state level decreases with increasing temperature because of a dynamic softening. In order to simulate the effect of static softening, the HPT-processed Pd disc at 573 K was held at the same corresponding temperature for 30 h. The hardness values are then plotted against the equivalent strain in Fig. 10(b). It is now apparent that a hardness maximum appears and the hardness level decreases due to a static softening. An orientation map by EBSD is shown in Fig. 11 for the steady state condition after annealing at 573 K for 30 h. The grain boundaries are smooth and straight, the grains are slightly elongated and the average grain size obtained by measuring the two orthogonal axes of the grains is ~1.4 μm. The feature appears to be typical of grains after annealing. A comparison of Figs. 2 and 11 indicates that the microstructures of Al and Pd are very similar at the homologous temperature of 0.32. The difference may be that whereas some elongated grains are observed in Pd as shown in Fig. 11, they are rarely seen in Al as in Fig. 2.

Therefore, the peak appearance for pure Al with straining by HPT must be due to static softening. However, the hardness decrease should be due to both dynamic and static softening. Inspection of Fig. 10(a) and (b) shows that the contribution of dynamic softening to the total softening using Eq. (2) is R_D = 38% for the Pd processed at 0.31 T_m. This R_D value for Pd is also included in Fig. 8. For comparison, the R_D value for Cu at the same homologous temperature is estimated to be 23%. This comparison indicates that the contribution of dynamic softening on the hardness decrease becomes more important as the SFE increases because the SFE is 45 mJ.m^{-2} for Cu and 180 mJ.m^{-2} for Pd [32]. It should be noted that neither the hardness peak nor the hardness decrease was observed in low purity Al (99.7%) [8]. The presence of impurity elements then

suppresses the recovery and recrystallization, stabilizes the microstructure and eliminates the softening after processing by HPT [37].

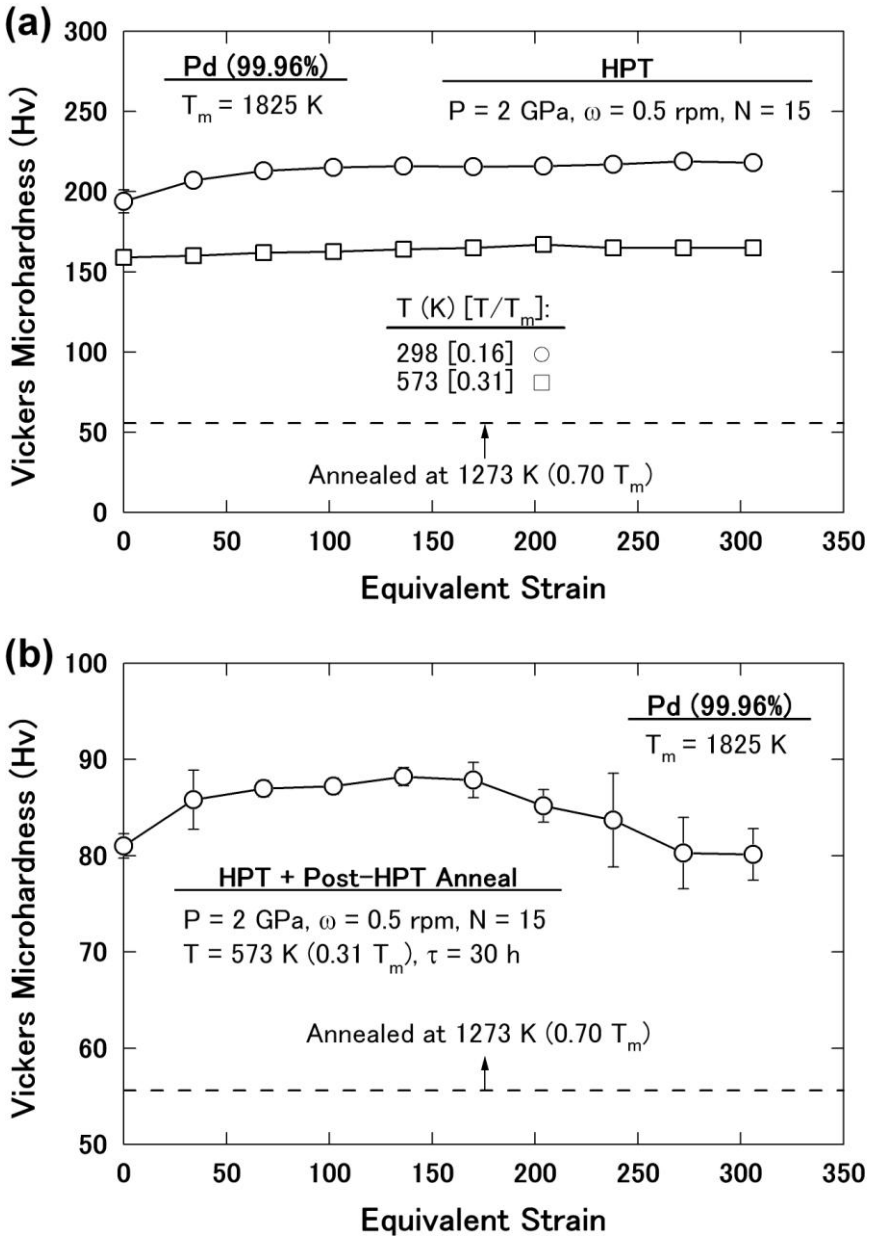

Fig. 10. Vickers microhardness plotted against equivalent strain for Pd after (a) HPT at room temperature and 573 K for 15 revolutions and (b) post-HPT annealing at 573 K for 30 h.

4.3. Hardness behavior at different homologous temperatures

Based on the hardness measurements, Fig. 12 illustrates the summary of the present results. It is thus clearly demonstrated that there are three distinct types of hardness behavior in pure metals. First, at low homologous temperatures as room temperature in Cu [20], Fe [21], Ti [22], Zr [23] and Hf [24], the hardness increases with an increase in the equivalent strain at an early stage of straining but levels off and enters into a steady state where the hardness remains unchanged with further

straining. Second, at moderate homologous temperatures as room temperature in Al [5,6,25–27], Mg [19] and Zn, the hardness initially increases with increasing strain and, after reaching a maximum, decreases to a steady level. Third, at high homologous temperatures as room temperature in Pb, Sn and In, the hardness remains almost unchanged or slightly decreases with an increase in the equivalent strain at an early stage of straining and enters into a steady state at large strains.

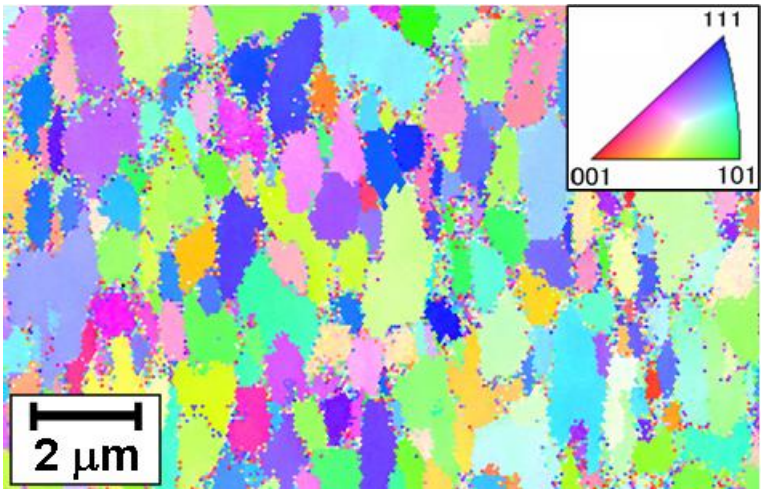

Fig. 11. EBSD orientation map for Pd after HPT processing for 15 revolutions at 573 K and post-HPT annealing at 433 K for 30 h.

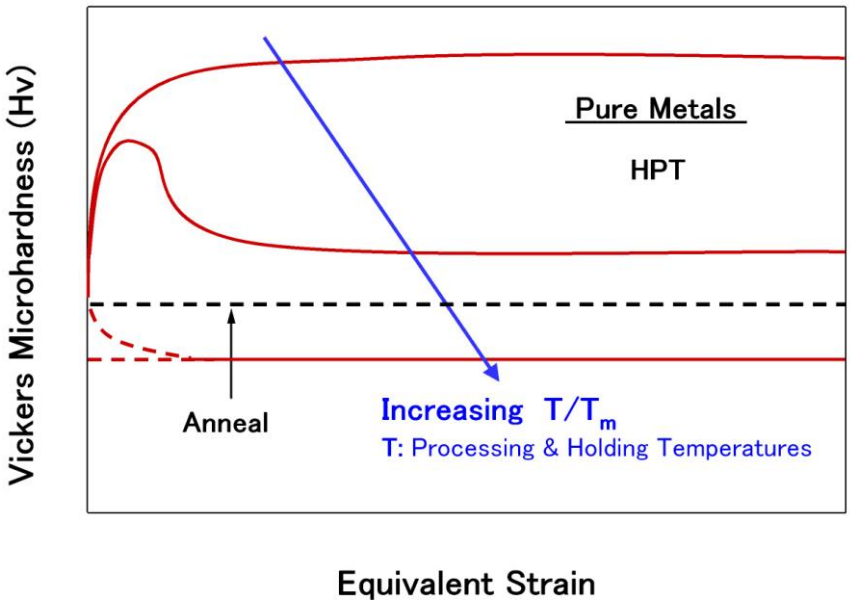

Fig. 12. Illustration of hardness behavior of pure metals after HPT for different homologous temperatures.

At high homologous temperatures, the hardness at the steady state by HPT decreases below the hardness level of the annealed samples despite a moderate decrease in the grain size after the HPT processing and this is against the Hall–Petch relationship. It should be noted that the Hall–Petch

relation is not valid at high homologous temperatures because of the effect of grain boundary sliding and the flow of vacancies. Thus, to clarify the reason for this decrease, the two additional measurements were carried out in this study. First, the hardness was measured on grain boundaries and grain interiors in Sn processed by HPT and compared with the average hardness, 6.9 Hv, in Fig. 5(b). It should be noted that the hardness values do not give the absolute hardness of grains and grain boundaries. However, since the indentation size is several times smaller than the grain size, a comparison between the two hardness measurements shows the effect of grain boundary. The hardness is 7.0 Hv in the grain interiors and 6.4 Hv on grain boundaries. Thus, the presence of grain boundaries can reduce the hardness in Sn.

Second, an HPT-processed In disc was annealed at 393 K for 1 h and its hardness was compared with the annealed sample prior to HPT. Following the annealing, the hardness of the HPT-processed disc increases from 1.4 Hv to 1.7 Hv which equals to the prior hardness of the annealed sample, 1.7 Hv. The results of these two experiments suggest that the lower hardness of the HPT-processed samples should be due to the contribution of grain boundaries which may act as a dislocation sink or cause grain boundary sliding to release strain hardening.

4.4. Effect of homologous temperature and stacking fault energy on grain size

Based on the hardness measurement and microstructural observation, it is clearly demonstrated that the homologous temperature and SFE are two important factors affecting the microstructural evolution in pure metals after HPT processing. On the one hand, the contribution of dynamic softening (R_D in Eq. (2)) increases with an increases in the homologous temperature and SFE. On the other hand, the dislocation mobility is high, and consequently, the static softening evolves much faster when the SFE is large [29]. However, close microstructural examinations indicate that although the SFE influence the microstructural evolution, the homologous temperature appears to be a more significant parameter influencing the steady-state grain size after processing by HPT.

Grain sizes at the steady state are plotted in Fig. 13 against the homologous temperature. The results reported for HPT-processed Ag (99.99%) and Au (99.999%) [38] are also included in Fig. 13 together with the result of an additional HPT experiment on Ni (99.996%) after 10 revolutions in this study. It should be noted that room temperature corresponds to homologous temperatures of 0.24 for Ag, 0.22 for Au and 0.17 for Ni. It is apparent that the average grain sizes at the steady state are well represented by a unique function of homologous temperature. The grain size at the steady state increases monotonically with an increase in the homologous temperature. Here, in order to examine the effect of SFE on the average grain size, the grain sizes at the steady state are plotted in Fig. 14 against SFE for some given homologous temperatures. The results reported for HPT-processed Ag (99.99%) and Au (99.999%) [38] as well as Ni (99.996%) are also included in Fig. 14. It should be noted that SFEs for Ag, Au and Ni are 16, 32 and 125 mJ m^{-2}, respectively [20]. It appears that the final grain size is almost independent of SFE and this contrasts well with the grain size dependence on homologous temperature. The present result of the negligible dependence of SFE on the final grain size in HPT-processed metals disagrees with the report by Mohamed [30] in ball-milled metals and with the report by Zhao et al. [39] in HPT-processed alloys

where the grain size decreases with decreasing SFE. It is important to note that the plots in Fig. 14 are made at given homologous temperatures for high purity metals. The contradiction arose because the effect of homologous temperature in Ref. [30] and the effect of solute atoms in Ref. [39] were not taken into account.

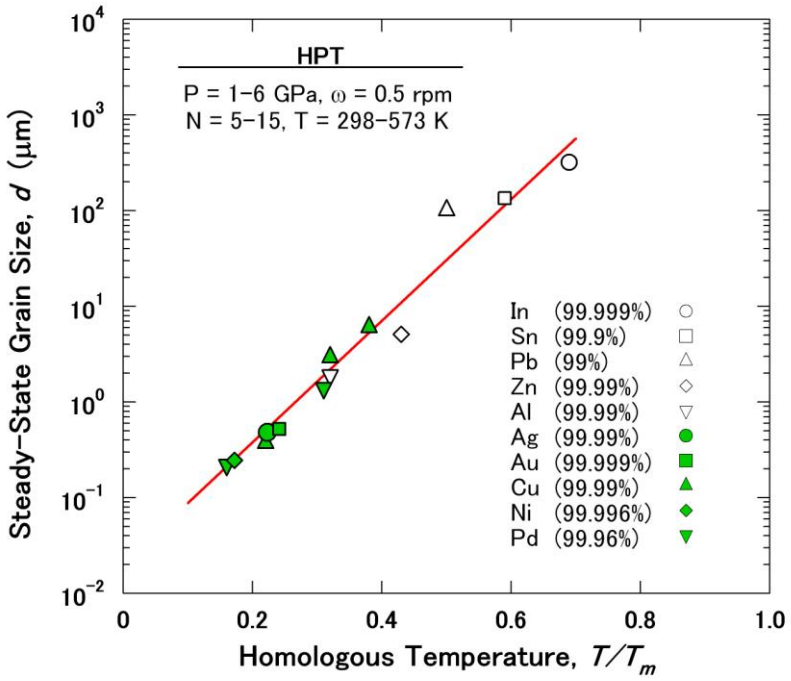

Fig. 13. Grain size at steady state, d, plotted against homologous temperature, T/Tm, for various pure metals. Data for Ag and Au were taken from Ref. [38].

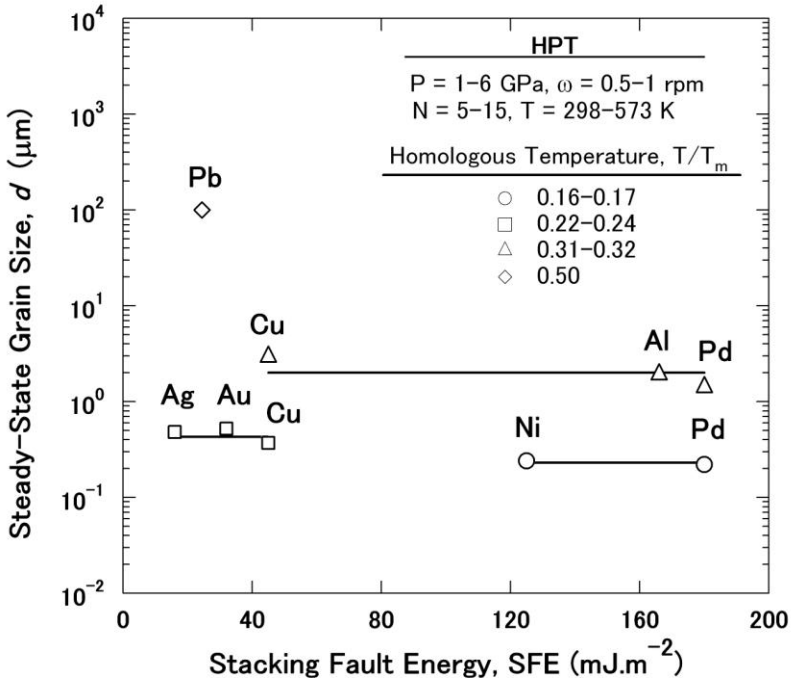

Fig. 14. Grain size at steady state, d, plotted against stacking fault energy, SFE, for various pure metals in various homologous temperatures. Data for Au and Ag were taken from Ref. [38].

5. Conclusions

High purity metals with low melting temperatures such as In, Sn, Pb, Zn and Al were processed using high-pressure torsion (HPT) and the following conclusions were obtained.

1. A peak appears in Al and Zn when their hardness values are plotted against equivalent strain.
2. Pure Cu and Pd were used to simulate a thermal effect on the softening. It was shown that the hardness peak appears as in Al by static softening after processing by HPT.
3. Despite a moderate grain refinement in Pb, Sn and In, the hardness level at the steady state attained by HPT decreases below the hardness level of the annealed sample prior to HPT. This may be due to the contribution of grain boundaries acting as a dislocation sink or causing grain boundary sliding to release strain hardening.
4. As the homologous temperature increases, dynamic softening becomes important to decrease the hardness at the steady state. The homologous temperature is a dominant parameter to determine the steady-state grain size of pure metals processed by HPT.
5. The stacking fault energy (SFE) affects the dislocation mobility and the dynamic softening occurs more quickly to reach the steady state. However, the grain size at the steady is independent of the SFE at a given homologous temperature.

Acknowledgements

One of the authors (KE) thanks the Islamic Development Bank (IDB) for a doctoral scholarship and the Japan Society for Promotion of Science (JSPS) for a postdoctoral scholarship. This work was supported in part by the Light Metals Educational Foundation of Japan, in part by a Grant-in-Aid for Scientific Research from the Ministry of Education, Culture, Sports, Science and Technology of Japan in the Innovative Area “Bulk Nanostructured Metals”, and in part by Kyushu University Interdisciplinary Programs in Education and Projects in Research Development (P&P).

References

[1] R.Z. Valiev, R.K. Islamgaliev, I.V. Alexandrov, Prog. Mater. Sci. 45 (2000) 103–189.
[2] R.Z. Valiev, Y. Estrin, Z. Horita, T.G. Langdon, M.J. Zehetbauer, Y.T. Zhu, J. Met. 58 (4) (2006) 33–39.
[3] A.P. Zhilyaev, T.G. Langdon, Prog. Mater. Sci. 53 (2008) 893–979.
[4] P.W. Bridgman, Phys. Rev. 48 (1935) 825–847.
[5] Y. Harai, Y. Ito, Z. Horita, Scripta Mater. 58 (2008) 469–472.
[6] Y. Ito, Z. Horita, Mater. Sci. Eng. A 503 (2009) 32–36.
[7] R.Z. Valiev, Y.V. Ivanisenko, E.F. Rauch, B. Baudelet, Acta Mater. 44 (1996) 4705–4712.
[8] A.P. Zhilyaev, T.R. McNelley, T.G. Langdon, J. Mater. Sci. 42 (2007) 1517–1528.
[9] A. Vorhauer, R. Pippan, Scripta Mater. 51 (2004) 921–925.
[10] M. Hafok, R. Pippan, Philos. Mag. 88 (2008) 1857–1877.
[11] M. Hafok, R. Pippan, Int. J. Mater. Res. 101 (2010) 1097–1104.
[12] A.P. Zhilyaev, S. Lee, G.V. Nurislamova, R.Z. Valiev, T.G. Langdon, Scripta Mater. 44 (2001) 2753–2758.

[13] Y. Todaka, Y. Miki, M. Umemoto, C. Wang, K. Tsuchiya, Mater. Sci. Forum 584–586 (2008) 597–602.
[14] B.J. Bonarski, E. Schafler, B. Milkulowskei, M.J. Zehetbauer, Mater. Sci. Forum 584–586 (2008) 263–268.
[15] A.V. Sergueeva, V.V. Stolyarov, R.V. Valiev, A.K. Mukhrjee, Scripta Mater. 45 (2001) 747–752.
[16] Y. Todaka, J. Sasaki, T. Moto, M. Umemoto, Scripta Mater. 59 (2008) 615–618.
[17] G. Khatibi, J. Horky, B. Weiss, M. Zehetbauer, Int. J. Fatigue 32 (2010) 269–278.
[18] X.Z. Liao, Y.H. Zhao, S.G. Srinivasan, Y.T. Zhu, R.Z. Valiev, D.V. Gunderov, Appl. Phys. Lett. 84 (2004) 592–594.
[19] K. Edalati, A. Yamamoto, Z. Horita, T. Ishihara, Scripta Mater. 64 (2011) 880–883.
[20] K. Edalati, T. Fujioka, Z. Horita, Mater. Sci. Eng. A 497 (2008) 168–173.
[21] K. Edalati, T. Fujioka, Z. Horita, Mater. Trans. 50 (2009) 44–50.
[22] K. Edalati, E. Matsubara, Z. Horita, Metall. Mater. Trans. A 40 (2009) 2079–2086.
[23] K. Edalati, Z. Horita, S. Yagi, E. Matsubara, Mater. Sci. Eng. A 523 (2009) 277–281.
[24] K. Edalati, Z. Horita, Y. Mine, Mater. Sci. Eng. A 527 (2010) 2136–2141.
[25] C. Xu, Z. Horita, T.G. Langdon, Acta Mater. 55 (2007) 203–212.
[26] M. Kawasaki, B. Ahn, T.G. Langdon, J. Mater. Sci. 45 (2010) 4583–4593.
[27] M. Kawasaki, T.G. Langdon, Mater. Sci. Eng. A 498 (2008) 341–348.
[28] K. Edalati, Z. Horita, J. Mater. Sci. 45 (2010) 4578–4582.
[29] K. Edalati, Y. Ito, K. Suehiro, Z. Horita, Int. J. Mater. Res. 100 (2009) 1668–1673.
[30] F.A. Mohamed, Acta Mater. 51 (2003) 4107–4119.
[31] A. Buch, Short Handbook of Metal Elements Properties and Elastic Properties of Pure Metals, 3rd ed., Krzysztof Biesaga, Warasaw, 2005.
[32] J.P. Hirth, J. Lothe, Theory of Dislocations, 2nd ed., McGraw-Hill, New York, NY, 1968.
[33] T. Jossang, J.P. Hirth, Philos. Mag. 13 (1966) 657–670.
[34] K. Edalati, Z. Horita, T.G. Langdon, Scripta Mater. 60 (2009) 9–12.
[35] Y. Iwahashi, Z. Horita, M. Nemoto, T.G. Langdon, Acta Mater. 46 (1998) 3317–3331.
[36] M. Kawasaki, Z. Horita, T.G. Langdon, Mater. Sci. Eng. A 524 (2009) 143–150.
[37] Z. Horita, Proceedings of the 12th International Conference on Aluminum Alloys, The Japan Institute of Light Metals, Yokohama, 2010, pp. 40–45.
[38] H. Matsunaga, Z. Horita, Mater. Trans. 50 (2009) 1633–1637.
[39] Y.H. Zhao, Y.T. Zhu, X.Z. Liao, Z. Horita, T.G. Langdon, Mater. Sci. Eng. A 410–411 (2005) 188–193.